VILNIUS TECH
Vilnius Gediminas Technical University

AVIATION
ISSN: 1648-7788 / eISSN: 1822-4180
2023 Volume 27 Issue 1: 14–26
https://doi.org/10.3846/aviation.2023.18498

A LAMINAR FLOW, PROPULSIVE, JET-FLAPPED CONCEPT FOR ELECTRICALLY POWERED TRANSPORT AIRCRAFT

Nikolaos KEHAYAS *

Department of Aeronautical Sciences, Hellenic Air Force Academy, 13671 Dekelia, Greece

Received 25 April 2022; accepted 17 August 2022

Abstract. Friction drag constitutes approximately half of the total drag of subsonic civil transport aircraft at cruise conditions. Several means were examined to control the flow over an aircraft and achieve laminar flow. Here, a new concept for friction drag reduction in the form of an integration of the aerodynamics and propulsion of the aircraft is put forward. Engines buried in the wing and at the rear of the fuselage suck the boundary layer of the entire wing and fuselage surface, and then, they used it as intake air and exhaust through ducts. At the wings, the engines exhaust in the form of a jet flap at the trailing edge providing distributed propulsion. By this laminar flow, propulsive concept laminar flow is established over the entire aircraft, resulting in substantial drag reduction. The analysis showed that out of the four electrically powered aircraft versions considered only the combined lift distribution with tailless fuselage is about to be feasible. It was also found that the example aircraft design is inappropriate. It is expected that a design purposely based on the proposed concept would bring electrically powered transport aircraft within the specific energy levels of present batteries.

Keywords: jet wing, drag reduction, laminar flow, hybrid laminar flow control (HLFC), boundary-layer suction, distributed propulsion, jet flap, electric aircraft.

Introduction

Fuel costs and greater awareness of the impact of emissions on the atmosphere raise the importance of energy efficiency for future transport aircraft. Fuel consumption can be reduced by decreasing airframe weight or drag and improving the efficiency of the propulsion system (Allison et al., 2010). At subsonic speeds aircraft drag is caused by two basic phenomena: the influence of viscosity, primary through skin friction, and losses associated with the generation of wing lift (Kroo, 2001). At cruise conditions friction drag constitutes about half of the total drag (Reneaux, 2004). Therefore, several means were examined to control the flow over an aircraft, and achieve to some degree laminar flow (Joslin, 1998).

The main concepts leading to laminar flow are laminar flow control (LFC), and its development hybrid laminar flow control (HLFC), and natural laminar flow (NLF). LFC is an active boundary-layer flow control (usually suction) technique employed to maintain the laminar state of flow at chord Reynolds number beyond that is normally characterized as being transitional or turbulent in the absence of control. NLF employs a favorable pressure gradient to delay the transition process. It is based on appropriate wing design. Inherent in practical NLF are aircraft of small or moderate size with low sweep wings. HLFC integrates the concepts of LFC with NLF to reduce system complexity. Suction is applied only in the leading-edge region of the wing and NLF is maintained over the rest of the wing through proper tailoring of the wing geometry (Joslin, 1998). In addition to different concepts, there are issues that transcend all concepts, such as boundary layer instabilities, surface tolerances, slot and hole suction schemes and insect, dirt, and ice contamination. Lack of wide LFC application lies on efficiency, reliability, and flight safety matters and, ultimately, on cost-benefit related to fuel prices (Joslin, 1998).

The idea of an integrated propulsion-lift system was first proposed by Kuchemann in 1947 (Attinello, 1957) as a "jet wing" configuration. This configuration incorporates the propulsion system by burying the engines in the wing and letting the engines exhaust out the trailing edge (Ko et al., 2003). Later, under the term "distributed propulsion", various similar concepts were proposed which involve engines distributed in the wingspan or engines, or fans, embedded in the wing exhausting through ducts along the entire trailing edge of the wing (Leifsson et al.,

*Corresponding author. E-mail: *n.kehayas@gmail.com*

2005; Kim et al., 2006; Schetz et al., 2010; Gohardani, 2013; Isikveren et al., 2014). Most distributed propulsion concepts were related to propulsion efficiency, especially those with boundary layer ingestion and wake filling (Smith & Roberts, 1947; Smith, 1993; Arntz & Atinault, 2015; Lv et al., 2016; Hall et al., 2017). Distributed propulsion not only provides propulsion but acts in many ways as an airframe and propulsion integration (Gohardani, 2013). Engines ingesting the wing and fuselage lower velocity boundary layer require less power and then, with their exhaust by filling the wake reduce drag. Among them is the combination of distributed propulsion with the jet flap. The jet flap (Davidson, 1956) is a flap in the form of a jet emerging out of the wing trailing edge. Although the jet flap was originally conceived as a high-lift device (Davidson, 1956), it was subsequently found to reduce also drag (Bowden et al., 1974; Chin et al., 1975; Bevilaqua et al., 1984). The distributed propulsion, jet flap scheme is about engines or fans embedded in the wing exhausting through fishtail ducts from jet flaps along the trailing edge of the wing (Kehayas, 2006). The result is not only improved propulsion efficiency and increased lift but also reduced drag, leading to a very high lift-to-drag ratio (Kim & Saunders, 2003; Kehayas, 2006; Kehayas, 2011b). In this sense it can be described as a jet wing, a propulsive wing, or an integrated aircraft (Attinello, 1957; Kehayas, 1986; Kehayas, 2011a). Here, a concept based on laminar flow through suction of the boundary layer and a distributed propulsion jet flap combination is being proposed. In this laminar flow, propulsive, jet-flapped concept the sucked boundary layer is used as incoming air by embedded engines in the wing and the fuselage to provide more efficient propulsion and filling the wing and fuselage wake. The engines buried in the wings exhaust in the form of a jet flap serving to increase lift-to-drag ratio. The concept includes Pfenninger and Groth (1961) scheme for laminar flow with boundary layer suction, the integrated aircraft (Kehayas, 2011a) and the jet flap (Davidson, 1956). The objectives are almost exactly the ones proposed by Kim and Saunders (2003), plus laminar flow. Namely: reduction in drag and weight by eliminating engine nacelles, reduction in drag through wing wake fill-in, increase in lift and reduction in drag due to the jet flap, additional lift during take-off and landing due to the jet flap, reduction in aircraft noise, improvement in safety due to multiple engines, elimination of aircraft control surfaces through differential and vectoring thrust for pitch, roll, and yaw, and laminar flow through suction (Pfenninger & Groth, 1961). The motivation is subsonic transport aircraft with very much higher lift-to-drag ratios, higher propulsive efficiency, and lower weight due to the integration of the aerodynamics with the propulsive system. However, due to the climatic change and the harmful effect of fossil fuels on the environment, the main motivation is that such improvements make feasible electrically powered large subsonic transport aircraft. The aim of this study is not to reach exact results but to put forward a laminar flow, propulsive, jet-flapped concept in principle.

1. Analysis

The proposed concept applied to wings is schematically shown in Figures 1 and 2. The boundary layer suction layout follows Pfenninger and Groth (1961). It consists of a glove in the shape of the chosen airfoil section with suction effectuated through a series of spanwise slots from 8 to 95% of the chord on both sides of the wing. The suction air passes across holes drilled into the inner part of the wing skin into individual suction chambers. At this point the proposed concept departs from the Pfenninger and Groth (1961) scheme. From the individual suction chambers, through appropriate nozzles, the boundary layer suction air is drawn by the embedded engines as intake air. Finally, the engines exhaust through fishtail ducts, from high-aspect-ratio two-dimensional nozzles located at a small flap, to flight speed as a jet flap along the entire trailing edge (Kehayas, 2011b).

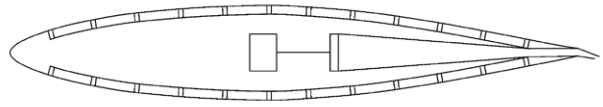

Figure 1. Schematic representation of the laminar flow, propulsive, jet-flapped concept applied to wings – system layout

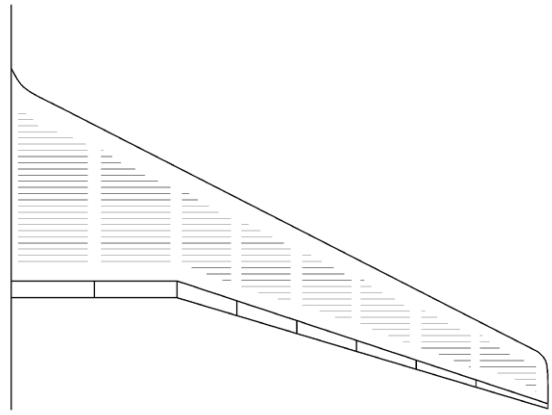

Figure 2. Schematic representation of the laminar flow, propulsive, jet-flapped concept applied to wings – top view

Following the analysis of Pfenninger and Groth (1961) the power balance equation (Drela, 2009) can be expressed as:

$$P_{WK} = \Phi_{w\infty} - F_X \cdot U_0, \tag{1}$$

where P_{WK} is the mechanical flow power for the wing, $\Phi_{w\infty}$ is the total wing energy dissipation and $-F_X U_0$ is the reversible energy outflow at the wing surface due to "excess thrust" (Hall et al., 2017).

For cruise at fixed altitude and velocity ($F_X = 0$) we have:

$$P_{WK} = \Phi_{ws} + \Phi_{ww} + \Phi_{wv} + \Phi_{wej}. \tag{2}$$

Power, P_{WK}, supplied by the engines to suck the wing boundary layer, and then, to accelerate the suction air to

flight speed, U_0, at the engine exit = Energy dissipation in the wing surface boundary layer, Φ_{ws} + Energy dissipation of the wing wake, Φ_{ww} + Energy dissipation of the wing vortices, Φ_{wv} + Energy dissipation of the engines jet, Φ_{wej}.

According to Pfenninger and Groth (1961) the power provided by the engine, P_{WK}, is:

$$P_{WK} = \frac{C_{DS} \cdot 1/2 \cdot \rho \cdot U_0{}^2 \cdot 2 \cdot S_N \cdot U_0}{\eta}, \quad (3)$$

where C_{DS} is the "equivalent drag" coefficient, ρ is the air density, S_N is the net (exposed) wing reference surface, U_0 is the flight speed (undisturbed flow velocity) and η is the efficiency of the system.

Following Pfenninger and Groth (1961), suction is applied from 8 to 95% of the chord. Hence, $2S_N$ is approximately the suction (wetted) wing area.

Furthermore (Lv et al., 2016; Hall et al., 2017):

$$\Phi_{ws} = b_N \cdot \rho \cdot U_0{}^3 \cdot k; \quad (4)$$

$$\Phi_{ww} = b_N \cdot \rho \cdot U_0{}^3 \cdot (2 \cdot \theta - k); \quad (5)$$

$$\Phi_{wv} = \frac{C_L{}^2 \cdot \frac{1}{2} \cdot \rho \cdot U_0{}^2 \cdot S \cdot U_0}{e \cdot \pi \cdot AR}; \quad (6)$$

$$\Phi_{wej} = \frac{1}{2} \cdot \dot{m}_w \cdot (U_j - U_0)^2, \quad (7)$$

where b_N is the net (exposed) wingspan, k is the kinetic thickness, θ is the momentum thickness, C_L is the lift coefficient, S is the wing reference area, ρ is the air density, e is the Oswald factor, AR is the wing aspect ratio, $\dot{m}_W$ is the mass flow rate and U_j is the engine jet velocity.

Following Pfenninger and Groth (1961), as the engines accelerate the suction air and exhaust it with a velocity, U_j, equal to flight speed, U_0, the energy dissipation of the engines jet, Φ_{wej}, is zero. Therefore,

$$\frac{C_{DS} \cdot 1/2 \cdot \rho \cdot U_0{}^2 \cdot 2 \cdot S_N \cdot U_0}{\eta} = b_N \cdot \rho \cdot U_0{}^3 \cdot k + b_N \cdot \rho \cdot U_0{}^3 \cdot (2 \cdot \theta - k) + \frac{C_L{}^2 \cdot \frac{1}{2} \cdot \rho \cdot U_0{}^2 \cdot S \cdot U_0}{e \cdot \pi \cdot AR} + 0. \quad (8)$$

In the evaluation of Eq. (8) the following assumptions and approximations were made:

1. The momentum and kinetic thicknesses refer to a flat plate.
2. The boundary layer of both sides of the wing – upper and lower – is considered.
3. An approximate three-dimensional approach was adopted, exemplified by the net wingspan, b_N.
4. An efficiency, η, for the whole system was proposed.
5. The velocity of the engines - jet flap jet was assumed constant across the jet.

Eq. (8) is solved for C_{DS}. All the other parameters are known. Exercising some manipulations, we have:

$$\frac{C_{DS} \cdot 2 \cdot S_N}{\eta} = 4 \cdot b_N \cdot \theta + \frac{C_L{}^2 \cdot S}{e \cdot \pi \cdot AR}; \quad (9)$$

$$C_{DS} = \frac{\eta}{2 \cdot S_N} \left(4 \cdot b_N \cdot \theta + \frac{C_L{}^2 \cdot S}{e \cdot \pi \cdot AR} \right). \quad (10)$$

Pfenninger and Groth (1961), Figure 7, p. 990 indicate a linear relation between weight flow coefficient, C_W, and "equivalent" drag coefficient, C_{DS}:

$$C_W = 0.65 \cdot C_{DS} + 0.5 \cdot 10^{-4}. \quad (11)$$

Combining Eqs (10) and (11) leads to:

$$C_W = 0.65 \cdot \left(\frac{\eta}{2 \cdot S_N} \left(4 \cdot b_N \cdot \theta + \frac{C_L{}^2 \cdot S}{e \cdot \pi A \cdot R} \right) \right) + 0.5 \cdot 10^{-4}. \quad (12)$$

and the mass flow rate, $\dot{m}_W$, according to Pfenninger and Groth (1961), is:

$$\dot{m}_W = C_W \cdot \rho \cdot U_0 \cdot 2 \cdot S_N. \quad (13)$$

Assuming flat plate conditions, the kinetic and momentum thicknesses are respectively:

$$k = 1.044 \cdot \left(\frac{\mu \cdot c_N}{\rho \cdot U_0} \right)^{1/2}; \quad (14)$$

$$\theta = 0.664 \cdot \left(\frac{\mu \cdot c_N}{\rho \cdot U_0} \right)^{1/2}, \quad (15)$$

where μ is dynamic viscosity and c_N is the mean net aerodynamic chord.

The proposed concept applied to fuselage is schematically shown in Figures 3 and 4. The boundary layer suction layout follows Pfenninger and Groth (1961). It consists of a glove in the shape of the fuselage with suction effectuated through a series of circumference slots along the length of the fuselage. The suction air passes across holes drilled into the inner part of the fuselage skin into individual suction chambers. At this point the proposed concept departs from the Pfenninger and Groth (1961) scheme. From the individual suction chambers through appropriate nozzles the boundary layer suction air passes into a common circumference suction duct running along the fuselage. This duct leads to the entry of an embedded engine located at the tail of the fuselage. The boundary layer suction air is drawn by the embedded engine as intake air. Finally, the engine exhausts through a tail nozzle to flight speed.

Figure 3. Schematic representation of the laminar flow, propulsive concept applied to fuselage – system layout

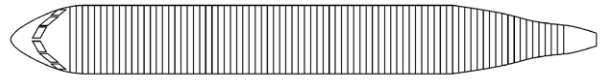

Figure 4. Schematic representation of the laminar flow, propulsive concept applied to fuselage – top view

Again, following the analysis of Pfenninger and Groth (1961) the power balance equation (Drela, 2009) can be expressed as:

$$P_{FK} = \Phi_{f\infty} - F_X \cdot U_0 . \quad (16)$$

The only difference is that the fuselage, in contrast to the wing, does not produce vortex dissipation. That is, Φ_{fv} = 0. And as the engines accelerate the suction air to flight speed, U_0, the energy dissipation of the engines jet, Φ_{fej} = 0. Therefore, power, P_{FK}, from the engine to suck the fuselage boundary layer and then, to accelerate the suction air to flight speed, U_0 = Energy dissipation in the fuselage surface boundary layer, Φ_{fs} + Energy dissipation of the fuselage wake, Φ_{fw}.

For cruise at fixed altitude and velocity (F_X = 0).

$$P_{FK} = \Phi_{fs} + \Phi_{fw} . \quad (17)$$

Therefore, taking into consideration the fuselage geometry we have:

$$\frac{C_{DS} \cdot 1/2 \cdot \rho \cdot U_0^2 \cdot S_F \cdot U_0}{\eta} = \pi \cdot d_m \cdot \rho \cdot U_0^3 \cdot k + \pi \cdot d_m \cdot \rho \cdot U_0^3 \cdot (2 \cdot \theta - k) . \quad (18)$$

In the evaluation of Eq. (16) the following assumptions and approximations were made:

- Following Pfenninger and Groth (1961), suction is applied from the end of the aircraft cockpit windscreen to 95% of the fuselage length;
- The momentum and kinetic thicknesses refer to a flat plate;
- An approximate three-dimensional approach was adopted, exemplified by the fuselage mean geometric diameter, d_m;
- An efficiency, η, for the whole system was proposed;
- The velocity of the engine exhaust jet was assumed constant across the jet.

With $d_m = S_F / (l\pi)$, where S_F is the fuselage surface, l the fuselage length and d_m is the fuselage mean geometric diameter. With some manipulations of Eq. (18), we have:

$$\frac{C_{DS}}{\eta} = \frac{4 \cdot \theta}{l} ; \quad (19)$$

$$C_{DS} = \eta \cdot \frac{4 \cdot \theta}{l} . \quad (20)$$

Using Eqs (11) and (20)

$$C_W = 0.65 \cdot \left(\eta \cdot \frac{4 \cdot \theta}{l} \right) + 0.5 \cdot 10^{-4} \quad (21)$$

and, as in Eq. (13), the mass flow rate, $\dot{m}_F$, is:

$$\dot{m}_F = C_W \cdot \rho \cdot U_0 \cdot S_F . \quad (22)$$

Assuming flat plate conditions and the length of the fuselage as the characteristic length, l, the kinetic and momentum thicknesses are respectively:

$$k = 1.044 \cdot \left(\frac{\mu \cdot l}{\rho \cdot U_0} \right)^{1/2} ; \quad (23)$$

$$\theta = 0.664 \cdot \left(\frac{\mu \cdot l}{\rho \cdot U_0} \right)^{1/2} . \quad (24)$$

2. Laminar flow, propulsive, jet-flapped concept benefit for transport aircraft

To establish the benefit of the concept for subsonic transport aircraft an example is needed. For this purpose, an aircraft design based on the Airbus A320neo will be used. The example aircraft specifications are shown in Table 1.

Table 1. Example aircraft specifications

Length (fuselage), l	37.57 m
Wingspan, b_N	35.80 m
Wing area, S	123 m^2
Aspect ratio, AR	10.42
Net (exposed) wing area, S_N	102 m^2
Net (exposed) wingspan, b_N	32 m
Mean net aerodynamic chord, c_N	3.187 m
Fuselage mean diameter, d_m	3.95 m
Fuselage wetted area, S_F	420 m^2
Maximum take-off mass	71,500 kg
Payload	14,850 kg
Operational empty mass	44,300 kg
Fuel	12,350 kg
Engines thrust	2 x 120 kN
Engines mass	2 x 3,000 kg
Cruising speed at 36,000 ft	M 0.78 (230 m/s)
Range	3,500 km
Level flight duration	3.6 h
Climb and descend duration	0.6 h

2.1. Laminar flow, propulsive, jet-flapped concept benefit for wings

To find the engine power required and the corresponding engine mass flow rate in applying the laminar flow, propulsive, jet-flapped concept to wings, numerical values are substituted in the power balance Eq. (8) and the mass flow rate Eq. (13). The calculations are performed in Appendix A. Results are:

Power, P_{WK}, supplied by the engines 1,432,976 W = Energy dissipation in the wing surface boundary layer, Φ_{ws}, 109,485 + Energy dissipation of the wing wake, Φ_{ww}, 29,774 W + Energy dissipation of the wing vortices, Φ_{wv}, 1,284,711 (A difference of 6 in the power balance equation is due to the accuracy of the calculations).

Engine mass flow rate $\dot{m}_{WC}$ = 28.8519 kg/s.

2.2. The jet flap effect

Consideration of the jet flap effect is beyond the scope of this study. However, it must be mentioned that the jet flap provides additional benefits in terms of increased lift,

reduced drag (Kim & Saunders, 2003) and almost total thrust recovery (Davidson, 1956). According to Kim and Saunders (2003) a jet flap can exhibit large lift coefficients and unusually negative drag coefficients at various flow conditions. These enhanced aerodynamics are caused by the trailing nozzle jet performing like virtual flap and by providing strong suction flow at the airfoil leading edge. Especially, drag coefficients can reach values as low as –0.25 (Kim & Saunders, 2003), Figure 5. The drag reduction realized by the jet flap is due to pressure forces. The negative drag is generated by a large suction force near the wing leading edge (Kim & Saunders, 2003). The lift and drag coefficients of Kim and Saunders (2003), Figure 5 are based on free stream conditions and the original untruncated NACA0012 airfoil chord length. They are calculated by integrating only the upper and lower airfoil surface pressure distributions without including the vectored jet (flap) force contribution to lift. Incorporating a jet flap into the laminar flow, propulsive, jet-flapped concept will add the exceptional pressure drag performance of the jet flap to the exceptional friction drag performance of laminar flow.

2.3. Combined elliptical and astroid hypocycloid lift distribution

Examining the magnitude of the terms of the power balance equation for wings (Appendix A, Eq. (A8)) it is evident that on the right-hand side of the equation by far the largest energy dissipation is due to wing vortices. It represents 90% of the total energy dissipation. It is therefore appropriate to take some measures to reduce it. Recently, a publication appeared proposing a new lift distribution for the reduction of induced drag. This lift distribution is a combination of an elliptical and an astroid hypocycloid distribution which when compared with the elliptical exhibits a 50% lower induced drag (Kehayas, 2021).

To find the engine power required and the corresponding engine mass flow rate in applying the laminar flow, propulsive, jet-flapped concept to wings with a combined elliptical and astroid lift distribution, numerical values are substituted in the power balance Eq. (8), taking into account the 50% reduction in induced drag, and the mass flow rate Eq. (13). The calculations are performed in Appendix B. Results are:

Power, P_{WCK}, supplied by the engines 781,610 W = Energy dissipation in the wing surface boundary layer, Φ_{wcs}, 109,485 + Energy dissipation of the wing wake, Φ_{wcw}, 29,774 W + Energy dissipation of the wing vortices, Φ_{wcv}, 642,355 (A difference of 4 in the power balance equation is due to the accuracy of the calculations).

Engine mass flow rate $\dot{m}_{WC}$ = 16.2231 kg/s.

2.4. Laminar flow, propulsive concept benefit for fuselage

To find the engine power required and the corresponding engine mass flow rate in applying the laminar flow, propulsive, concept to fuselage, numerical values are substituted in the power balance Eq. (18) and the mass flow rate Eq. (22). The calculations are performed in Appendix C. Results are:

Power, P_{FK}, supplied by the engines 167,015 W = Energy dissipation in the fuselage surface boundary layer, Φ_{fs}, 131,306 + Energy dissipation of the fuselage wake, Φ_{fw}, 35,715 W (A difference of 6 in the power balance equation is due to the accuracy of the calculations).

Engine mass flow rate $\dot{m}_F$ = 5.0474 kg/s.

The power balance numerical results of Appendices A to C are presented in Table 2. In the energy dissipation – power columns two cases are presented: in the left for the elliptical wing lift distribution and fuselage, and in the right for the combined wing lift distribution and fuselage. The power balance method (Drela, 2009) does not lend itself to an evaluation of interference drag. Therefore, a 5% due to interference (Torenbeek, 2013) is added to the final results of Table 2.

Table 2. Power balance for aircraft based on the example design at cruising conditions

Energy dissipation of aircraft constituent parts at Mach 0.78 and 36,000 ft	Energy dissipation – power / W	
Energy dissipation in the wing surface boundary layer, elliptical lift distribution	109,485	–
Energy dissipation in the wing wake, elliptical lift distribution	29,774	–
Energy dissipation of the wing vortices, elliptical lift distribution	1,284,711	–
Wing energy dissipation, elliptical lift distribution	1,423,970	–
Energy dissipation in the wing surface boundary layer, combined lift distribution	–	109,485
Energy dissipation in the wing wake, combined lift distribution	–	29,774
Energy dissipation of the wing vortices, combined lift distribution	–	642,355
Wing energy dissipation, combined lift distribution	–	781,614
Energy dissipation in the fuselage surface boundary layer	131,306	131,306
Energy dissipation in the fuselage wake	35,715	35,715
Fuselage energy dissipation	167,021	167,021
Energy dissipation of the engines jet, $U_j = U_0$	0	0
Aircraft (total) energy dissipation, wing with elliptical lift distribution and fuselage	1,590,991	–
Aircraft (total) energy dissipation, wing with combined lift distribution and fuselage	–	948,635

End of Table 2

Energy dissipation of aircraft constituent parts at Mach 0.78 and 36,000 ft	Energy dissipation – power / W	
Power supplied by the engines for wing with elliptical lift distribution and fuselage, system efficiency 80%	1,988,739	–
Power supplied by the engines for wing with elliptical lift distribution and fuselage, system efficiency 80% plus 5% interference drag	2,088,176	–
Power supplied by the engines for wing with combined lift distribution and fuselage, system efficiency 80%	–	1,185,794
Power supplied by the engines for wing with combined lift distribution and fuselage, system efficiency 80% plus 5% interference drag	–	1,245,084

The above values represent the power of engines working at 70% of their maximum at cruising conditions.

3. Evaluation of the specific energy and the specific power of the electric energy storage system

The concept applies to both gas turbines and electric motors with ducted fans as engines. But, as already stated in the introduction, due to the importance of achieving electrically powered large transport aircraft only electric motors with ducted fans will be addressed.

The results of Table 2 do not include a tail contribution for two reasons. The first was that according to Kim and Saunders (2003) and Kehayas (1986, 2006, 2011b) aircraft control surfaces could be eliminated through differential and vectoring thrust for pitch, roll, and yaw control. The second was the large number of calculations. To establish the benefit of the concept for large transport aircraft four versions will be considered. They are:

- Aircraft with elliptical wing lift distribution and fuselage without a tail (AC/WE + F).
- Aircraft with elliptical wing lift distribution and fuselage with a tail (AC/WE + F + T).
- Aircraft with combined wing lift distribution and fuselage without a tail (AC/WC + F).
- Aircraft with combined wing lift distribution and fuselage with a tail (AC/WC + F + T).

As with the example aircraft based on the Airbus A320neo, an example electric motor with ducted fan is proposed based on the Emrax 288 electric motor. The electric motor specifications are shown in Table 3. The size of the motor is an "average" appropriate for its embedment in the wing at the spanwise position of the geometric mean chord defined by the net (exposed) wing surface. It is meant for calculation purposes and, evidently, smaller, or larger motors will be used at other locations in the wings, fuselage, and tail.

Table 3. Example electric motor specifications

Cooling medium	Air
Mass	20 kg
Diameter/width	268/91 mm
Maximum battery voltage and maximum load RPM	250 Vdc – 4500 RPM
Peak motor power	200 kW
Continuous motor power	86 kW
Maximum motor torque	500 Nm
Continuous motor torque	200 Nm
Motor efficiency	92–98%
Controller efficiency	98%

To investigate the feasibility of electrically powered transport aircraft, the specific energy and the specific power capability of the electric energy storage system must be confirmed.

3.1. Evaluation of the specific energy of the electric energy storage system

In the evaluation of the required specific energy the following approximations and assumptions were made:

1. The duration of level flight is 3.6 hours (Table 1).
2. The duration of climb and descend is 0.6 hours (Table 1).
3. Power produced by electric motors with ducted fans is a function of air density.
4. During level flight the electric motor operates at 70% of its maximum continuous power (This is the design point for minimum specific fuel consumption for a gas turbine engine (Bensel, 2018)). It is applied to an electric motor for comparison purposes. In addition, it provides the necessary thrust margin for climb, descend and maneuvers)
5. During climb and descend the electric motor may operate up to 100% of its maximum continuous power or, even, for a few minutes close to peak power
6. For calculation purposes it is assumed that during climb and descend the altitude is the average of sea level and 36,000 ft which is = 18,000 ft (ρ = 0.6981 kg/m^3)

The energy consumed by the engines during the flight is made of the power supplied by the engines (70% of maximum continuous power in cruising conditions) times the duration of level cruising flight plus the power supplied by the engines (maximum continuous power) times the duration of climb and descend. In versions with a tail, a 35% of the power needed for wings is added (For large transport aircraft tail drag is 30–35% of wing drag (Howe, 2000)). Therefore:

For the two tailless versions, AC(WE + F) and AC(WC + F).

Energy = Power for level cruising flight (Table 2) times the duration of level cruising flight (3.6 h – Table 1) + Power for climb and descend (= 100/70 of Power for level cruising flight adjusted for flight at an average of 18,000 ft

(x 0.6981/0.3652)) times the duration of climb and descend (0.6 h – Table 2).

And for the two versions with tail, AC(WE + F + T) and AC(WC + F + T).

Energy = Power for level cruising flight (including an added 35% of the power for wings as contribution of the tail) (Table 2) times duration of level cruising flight (3.6 h – Table 1) + Power for climb and descend (= 100/70 of Power for level cruising flight adjusted for flight at an average of 18,000 ft (x 0.6981/0.3652) times duration of climb and descend (0.6 h – Table 1). The calculations are performed in Appendix D. Results are:

1. Energy consumed by AC(WE+F) = 10,938,764 Wh.
2. Energy consumed by AC(WE+F+T) = 13,549,539 Wh.
3. Energy consumed by AC(WC+F) = 6,522,283 Wh.
4. Energy consumed by AC(WC+F+T) = 7,955,334 Wh.

To find the specific energy, the mass of the electric energy storage system is needed. And for an electrically powered transport aircraft with the specifications of the example aircraft (Table 1) the mass of its electric energy storage system must correspond to the fuel mass of the example aircraft taking into account the total energy conversion chain efficiency (Hepperle, 2012). Using values of Table 3 for motor (0.95) and controller (0.98) efficiency, assuming that a gearbox is redundant in the case of a ducted fan (1.0) and ducted fan efficiency of 0.85 (Jin et al., 2018; Jia et al., 2021) leads to an electric system efficiency of 0.79. The fuel mass of the example aircraft is 12,350 kg (Table 1). That is, 0.79 12,350 = 9,756 kg is the effective corresponding mass of the electric storage system. According to the calculations performed in Appendix D the specific energy of the electric energy storage system must be:

- Specific energy for AC(WE + F) = 1,121 Wh/kg.
- Specific energy for AC(WE + F + T) = 1,389 Wh/kg.
- Specific energy for AC(WC + F) = 668 Wh/kg.
- Specific energy for AC(WC + F + T) = 815 Wh/kg.

3.2. Evaluation of the specific power of the electric energy storage system

The specific power required of the electric energy storage system of an electrically powered aircraft with the specifications of Table 1 is found by dividing the maximum take-off power required at sea level (ρ = 1.225 kg/m^3) by the example aircraft fuel mass (12,350 kg – Table 1). Maximum take-off power needed at sea level is, usually, the maximum power of any flight condition and fuel mass of example aircraft corresponds to electric storage system mass.

For the two tailless versions, AC(WE + F) and AC(WC + F).

Maximum power at sea level = Maximum power for cruising flight at 36,000 ft – ρ = 0.3652 kg/m^3 (Table 2) (= 100/70 of Power for level cruising flight, adjusted to sea level (x 1.225/0.3652)).

And for the two versions with tail, AC(WE + F + T) and AC(WC + F + T).

Maximum power at sea level = Maximum power for cruising flight at 36,000 ft – ρ = 0.3652 kg/m^3 (Table 2) including an added 35% of the power for wings as a contribution of the tail) (= 100/70 of power for level cruising flight including an added 35% of the power for wings as contribution of the tail, adjusted to sea level (x 1.225/0.3652)). The calculations are performed in Appendix E. Results are:

1. Maximum power required by AC(WE+F) = 10,006,320 W.
2. Maximum power required by AC(WE+F+T) = 12,409,644 W.
3. Maximum power required by AC(WC+F) = (100/70)· 1,245,084 · (1.225/0.3652) = 5,966,312 W.
4. Maximum power for AC(WC+F+T) = (100/70)· (1,245,084 + 0.35 · 781,614) · (1.225/0.3652) = 7,277,225 W.

Consequently, according to calculations performed in Appendix E the specific power of the electric energy storage system must be:

1. Specific power for AC(WE + F) = 810 W/kg.
2. Specific power for AC(WE + F + T) = 1,005 W/kg.
3. Specific power for AC(WC + F) = 483 W/kg.
4. Specific power for AC(WC + F + T) = 589 W/kg.

4. Mass estimation of electric motors

The mass of the electric motors (aircraft engines) is the maximum power required divided by the specific power of the "average" example electric motor (Table 3). The maximum continuous power of the example electric motor is 86,000 W and its mass is 20 kg (Table 3). To the mass of the electric motor a 30% is added accounting for items of the power train (controller, cables, cooling etc.) (Kammermann et al., 2020) leading to an overall electric motor mass of 26 kg and an electric motor specific power of 86,000/26 = 3,308 W/kg. The calculations are performed in Appendix F. Results are:

1. Mass of electric motors of AC(WE+F) = 3,025 kg.
2. Mass of electric motors of AC(WE+F+T) = 3,751 W/kg.
3. Mass of electric motors of AC(WC+F) = 1,804 W/kg.
4. Mass of electric motors of AC(WC+F+T) = 2,200 W/kg.

5. Results and discussion

For large electrically powered transport aircraft to be feasible, either the specific energy of the electric energy storage system must be increased or a breakthrough in aeronautical technology be achieved. With electrical storage system specific energy capacity at its present and foreseeable level, only laminar flow can attain this goal.

As stated in the introduction, the aim of this study is not to reach exact results but to put forward a laminar flow, propulsive, jet-flapped concept in principle. Evidently, a detailed study is needed, especially on the electric side of the design. However, it is claimed that the assumptions and approximations made, such as flat plate conditions for momentum thicknesses and an efficiency of 0.80 for the whole system, will not differentiate much the results a more exact study would obtain. The same holds for several design issues, like the additional weight of the ducting

mechanism and engines of smaller size and lower weight. From the aerodynamic point of view the results of the analysis are quite good. Among other, they exhibit a ratio of energy dissipation of wing wake, representing pressure drag, to energy dissipation of wing surface boundary layer, representing friction drag, of 0.26.

The concept is founded on the work of Pfenninger and Groth (1961). This work in not just theoretical and experimental. It is the outcome of flight tests in real conditions. In an operational aircraft, the fighter F-94A, by means of boundary layer suction laminar flow over the entire wing was achieved for Mach and Reynolds numbers of 0.7 and 35 million respectively. These flight conditions are close to those encountered by large transport aircraft. The fact that a fighter aircraft was used in the flight tests does not invalidate Pfenninger and Groth (1961) scheme's application to transport aircraft. In respect to boundary layer characteristics a fighter does not differ from a transport design (Kehayas, 1992; Fielding & Kehayas, 2000; Kehayas, 2007). From what it is known, Pfenninger and Groth's scheme (1961) is the only one to accomplish laminar flow over the entire wing (full chord) at such high Reynolds numbers in real operational conditions (Joslin, 1998). This result must be attributed to the main difference to similar schemes, which is the use of spanwise suction slots and not holes along the full and not part of the wing chord. Earlier, a theoretical treatment of the subject has been carried out by Smith and Roberts (1947).

In the proposed laminar flow, propulsive, jet-flapped concept, Pfenninger and Groth's scheme (1961) is coupled to the engines to form a propulsive wing (Attinello, 1957) and fuselage, known lately as distributed propulsion (Gohardani et al., 2011). Boundary layer suction air is drawn by the embedded in the wing and fuselage engines as intake air. Mass flow rates of around 28.85 and 5.05 kg/s (Appendix A Eq. (A12) and Appendix C Eq. (C12)) for wings and fuselage clearly indicate the suitability of coupling the engines to boundary layer suction. The coupling of the boundary layer suction to the engines goes beyond an integration of aerodynamics and propulsion. Using a control volume approach, the velocity of the incoming through suction slots air into the engines in the direction of flight is very small. The velocity of the incoming through suction air is perpendicular to the wing upper and lower surface. Thus, most of it is perpendicular to the direction of flight, and only a small part around the leading edge of the wing has a component in the direction of flight. The same conditions apply to the fuselage. The exhaust velocity of the engines set at flight speed minus the very small component of the velocity of the incoming through suction air leads to a change in momentum, and hence thrust, in a most efficient propulsive manner. The velocity of the incoming through suction air in the direction of flight can be calculated by equating the thrust power of the engines to the wing and fuselage energy dissipation. Assuming full nozzle expansion: $U_0 = \left(\dot{m}_W + \dot{m}_F\right)\left(U_0 - U_{in}\right)U_0 = \Phi_W + \Phi_F$. Using Appendix A Eqs (A8), (A12), and Appendix C Eqs (C8), (C12) we have: $(28.8519 + 5.0474)(230 - U_{in})230 = 1{,}423{,}970 + 167{,}02$ resulting in a, at maximum, component of velocity in the direction of flight of the incoming through suction air $U_{in} = 25.944$ *m/s*. Although the engines exhaust speed equals the flight speed, thrust is produced. In a way, it is like the workings of a rocket engine. And when the speed of the rocket equals the speed of the rocket engine exhaust gas the propulsive efficiency of the rocket engine is 100% (Houghton & Brock, 1970). Moreover, the concept is even more efficient because when the engine exhaust speed equals the flight speed, then, the energy dissipation of the wing and fuselage engines' jet is zero. A similar concept is boundary layer ingestion, in which some or all the aircraft wing or fuselage boundary layers are ingested by the engines and re-accelerated, instead of passing undisturbed into wakes (Hall et al., 2017). It provides higher propulsive efficiency due to reduced velocity of flow entering the engines compared with conventionally placed engines under the wings. But it is clearly inferior to the proposed concept because the velocity of the ingested air into the engines in the direction of flight is just reduced and not very small compared with engine exhaust speed.

The jet flap component of the proposed concept applied to wings is beyond the scope of this study. However, joining the proposed laminar flow, propulsive concept to a jet flap would greatly enhance drag reduction as jet-flapped wing drag coefficients can reach values as low as –0.25 (Kim & Saunders, 2003). It should be underlined that the drag reduction realized by the jet flap is due to pressure forces. The negative drag is generated by a large suction force near the wing leading edge (Kim & Saunders, 2003). Incorporating a jet flap into the laminar flow, propulsive concept will add the exceptional pressure drag performance of the jet flap to the exceptional friction drag performance of laminar flow. Lift coefficients of jet-flapped wings are as high as would be expected of a flap at an equivalent deflection angle. Kim and Saunders' work (2003) is supported either directly by Chin et al. (1975) and Kim et al. (2006) or indirectly as thrust recovery by Garland (1964), Davidson (1956) and Bevilaqua et al. (1984) among others. Research by Schetz et al. (2010) does not exactly reach the same conclusions. Some negative drag - thrust recovery over 100% – is observed but not to the extent shown by Kim and Saunders (2003). This may be due to different angle of attack and deflection angle of jet flap (0 and over 30 (Kim & Saunders, 2003) and 2.66 and 5 – 10 (Schetz et al., 2010) degrees respectively). In any case, a jet flap would considerably improve the performance of the proposed concept. A further advantage of the proposed concept is that it essentially keeps the "tube and wings" configuration and avoids complex designs such as the blended wing-body which offer few advantages and many disadvantages (Kehayas, 1998).

The results for the specific energy and the specific power of the electrical energy storage system, and the mass of the required electric motors including powertrain

Table 4. Specific energy of the electric energy storage system, specific power of the electric energy storage system and mass of the electric motors including powertrain mass for the four aircraft versions

Parameter	AC(WE + F)	AC(WE + F + T)	AC(WC + F)	AC(WC + F + T)
Specific energy of electric energy storage system, Wh/kg	1,121	1,389	668	815
Specific power of electric energy storage system, W/kg	810	1,005	483	589
Mass of electric motors, kg	3,025	3,751	1,804	2,200

mass for the four selected aircraft versions satisfying the specifications of the example large transport aircraft (Table 1), Aircraft with elliptical wing lift distribution and fuselage without a tail (AC/WE + F), Aircraft with elliptical wing lift distribution and fuselage with a tail (AC/WE + F + T), Aircraft with combined wing lift distribution and fuselage without a tail (AC/WC + F) and Aircraft with combined wing lift distribution and fuselage with a tail (AC/WC + F + T), are shown collectively in Table 4.

Regarding the specific power of the electrical storage system all four versions (Table 4) fall within the present technology level of batteries (Hepperle, 2012; Kammermann et al., 2020; Bolam et al., 2020). In all four versions the mass of the electric motors, including the mass of the powertrain (Table 4), is considerably less than the 6,000 kg mass of the example aircraft turbofan engines (Table 1). What remains to be examined is the specific energy of the electric energy storage system. The best current performance of battery specific energy capability is with Lithium-Sulphur batteries at nearly 500, and what is about to be achieved is 600 Wh/kg (The Faraday Institution, 2020; OXIS Energy, 2020). Projections in the near future vary between 700 and 1,250 Wh/kg (The Faraday Institution, 2020; Hepperle, 2012). As shown in Table 4 the specific energy requirements of the electrical storage system of the four versions lie between 668 and 1,389 Wh/kg. Hence, only the aircraft with combined wing lift distribution and fuselage without a tail (AC/WC + F) demanding a specific energy 668 Wh/kg is close to be about feasible. There are design complications with this tailless version, notably those of aircraft stability and control, but they can be addressed (Kim & Saunders, 2003). Nevertheless, the matter does not end here. The provision of a jet flap would certainly bring down the specific energy requirement for all four versions and specifically for the aircraft with combined wing lift distribution and fuselage without a tail to the present level of specific energy of Lithium-Sulphur batteries. Finally, although in principle the laminar flow, propulsive, jet-flapped concept benefit for electrically powered transport aircraft is valid, the results of the present study are partly inappropriate. This is evident from the enormous energy dissipation of the wing vortices compared with the sum of the energy dissipation of the wing surface boundary layer and the wing wake (Appendix A Eq. (A8)). The condition for maximum range for an electrically powered transport aircraft is that induced drag equals zero lift drag (friction drag plus pressure drag) (Hepperle, 2012). Hence, the energy dissipation of the wing vortices, representing induced drag, should be equal to the sum of energy dissipation of wing surface boundary layer, representing friction drag, and energy dissipation of wing wake, representing pressure drag. In this case the lift coefficient should be considerably smaller. Therefore, the wing surface area must respectively be much larger for the wing to generate the same lift. A much smaller lift coefficient will lead to substantially reduced energy dissipation of the wing vortices, which in turn will result in lower specific energy requirements of the electric energy storage system. But a much larger wing surface area would require an altogether different overall aircraft design. Consequently, the example aircraft design is unsuitable, and a new aircraft design is needed. It is expected that a design purposely based on the proposed laminar flow, propulsive, jet-flapped concept would bring electrically powered large transport aircraft within the specific energy levels of present batteries.

Conclusions

The main conclusion is that the proposed laminar flow, propulsive, jet-flapped concept can reduce drag to a degree that renders electrically powered large transport aircraft of typical range, having electric motors driving ducted fans as engines and cutting-edge technology batteries as energy storage system, feasible. The concept is founded on research carried out with an operational aircraft in real flight conditions. Through boundary layer air suction by the engines, laminar flow over the entire aircraft is achieved for Mach and Reynolds numbers typical of transport aircraft. The analysis showed that of the four aircraft versions considered, with elliptical or combined wing lift distribution and fuselage with or without tail, only the combined lift with tailless fuselage is at present about to be feasible. This borderline outcome is due to the present capacity of electric storage systems. Regarding the specific power, all four aircraft versions are within the current technology level of batteries. It was made evident in the analysis that 90% of the total drag is induced. Therefore, the example aircraft design is inappropriate, and a design purposely based on the proposed laminar flow, propulsive, jet-flapped concept is required.

Disclosure statement

The author declares not to have any financial, professional, personal interest or benefit arising from the direct application of his research.

References

Allison, E., Kroo, I., Sturdza, P., Suzuki, Y., & Martins-Rivas, H. (2010). Aircraft conceptual design with natural laminar flow. In *Proceedings of the 27th International Congress of Aeronautical Sciences* (pp. 1–9). Nice, France.

Arntz, A. & Atinault, O. (2015). Exergy-based performance assessment of a blended wing-body with boundary-layer ingestion. *AIAA Journal, 53*(12), 3766–3776. https://doi.org/10.2514/1.J054072

Attinello, J. S. (1957). The jet wing. In *IAS 25th Annual meeting.* Los Angeles, California, Preprint No. 703.

Bensel, A. (2018). *Characteristics of the specific fuel consumption for jet engines*. Project, Department of Automotive and Aeronautical Engineering, Hamburg University of Applied Science. https://doi.org/10.15488/4316

Bevilaqua, P. M., Schum, E. F., & Woan, C. J. (1984). Progress towards a theory of jet-flap thrust recovery. *Journal of Fluid Mechanics, 141,* 347–364. https://doi.org/10.1017/S0022112084000884

Bolam, R. C., Vagapov, Y., & Anuchin, A. (2020). A review of electrical motor topologies for aircraft propulsion. In *55th International Universities Power Engineering Conference (UPEC)* (pp. 1–6). Turin, Italy. https://doi.org/10.1109/UPEC49904.2020.9209783

Bowden, M. K., Renshaw, J. H., & Sweet, H. S. (1974). Propulsion integration for a hybrid propulsive-lift system. In *SAE Technical Paper 740471,* 1–12. SAE Mobilus. https://doi.org/10.4271/740471

Chin, Y.-T., Aiken, T. N., & Oates, G. S. (1975). Evaluation of a new jet flap propulsive-lift system. *Journal of Aircraft, 12*(7), 605–610. https://doi.org/10.2514/3.59841

Davidson, I. M. (1956). The jet flap. *The Aeronautical Journal, 60*(541), 25–50. https://doi.org/10.1017/S0368393100132389

Drela, M. (2009). Power balance in aerodynamic flows. *AIAA Journal, 47*(7), 1761–1771. https://doi.org/10.2514/1.42409

Fielding, J. P., & Kehayas, N. (2000). Design synthesis and optimization of an advanced short take-off and vertical landing (ASTOVL) combat aircraft. In *Proceedings of the 22nd International Congress of Aeronautical Sciences* (pp. 1–12). Harrogate, United Kingdom.

Garland, D. B. (1964). Jet flap thrust recovery: Its history and experimental realization. In *Proceedings of the AIAA/CASI Joint Conference* (pp. 1–9). Ottawa, Canada. https://doi.org/10.2514/6.1964-797

Gohardani, A. S., Doulgeris, G., & Singh, R. (2011). Challenges of future aircraft propulsion: A review of distributed propulsion technology and its potential application for the all electric commercial aircraft. *Progress in Aerospace Sciences, 47*(5), 369–391. https://doi.org/10.1016/j.paerosci.2010.09.001

Gohardani, A. S. (2013). A synergistic glance at the prospects of distributed propulsion technology and the electric aircraft concept for future unmanned air vehicles and commercial/military aviation. *Progress in Aerospace Sciences, 57,* 25–70. https://doi.org/10.1016/j.paerosci.2012.08.001

Hall, D. K., Huang, A. C., Uranga, A., Greitzer, E. M., Drela, M., & Sato, S. (2017). Boundary layer ingestion propulsion benefit for transport aircraft. *Journal of Propulsion and Power, 33*(5), 1118–1129. https://doi.org/10.2514/1.B36321

Hepperle, M. (2012). Electric flight – Potential and limitations. In *NATO AVT-209 Workshop on Energy Efficient Technologies and Concepts,* Technical Report STO-MP-AVT-209 (pp. 9–1, 9–30). Braunschweig, Germany.

Houghton, E. L., & Brock, A. E. (1970). *Aerodynamics for engineering students* (2nd ed.). Edward Arnold Publishers Limited.

Howe, D. (2000). *Aircraft conceptual design synthesis*. Professional Engineering Publishing Limited. https://doi.org/10.1002/9781118903094

Isikveren, A. T., Seitz, A., Bijewitz, J., Hornung, M., Mirzoyan, A., Isyanov, A., Godard, J.-L., Stückl, S., & van Toor, J. (2014). Recent advances in airframe-propulsion concepts with distributed propulsion. In *Proceedings of the 29th International Congress of Aeronautical Sciences* (pp. 1–14). St. Petersburg, Russia.

Jia, Y., Li, J., & Wu, J. (2021). Power fan design of blended-wing-body aircraft with distributed propulsion system. *International Journal of Aerospace Engineering,* 1–18. https://doi.org/10.1155/2021/5128136

Jin, Y., Qian, Y., Zhang, Y., & Zhuge, W. (2018). Modeling of ducted-fan and motor in an electric aircraft and a preliminary integrated design. *SAE International Journal of Aerospace, 11*(2), 115–126. https://doi.org/10.4271/01-11-02-0007

Joslin, R. D. (1998). *Overview of laminar flow control*. NASA TP-208705.

Kammermann, J., Bolvashenkov, I., Tran, K., Herzog, H.-G., & Frenkel, I. (2020). Feasibility study for a full-electric aircraft considering weight, volume, and reliability requirements. In *2020 International Conference on Electrotechnical Complexes and Systems (ICOECS)* (pp. 1–6). Ufa, Russia. https://doi.org/10.1109/ICOECS50468.2020.9278461

Kehayas, N. (1986). *The controlled propulsive wing*. United Kingdom Patent Office, UK Patent GB2167831 B, 1988.

Kehayas, N. (1992). *ASTOVL combat aircraft design synthesis and optimization* (Report No 9201). Cranfield University.

Kehayas, N. (1998). The blended wing-body configuration as an alternative to conventional subsonic civil transport aircraft design. In *Proceedings of the 21st International Congress of Aeronautical Sciences* (pp. 1–7). Melbourne, Australia.

Kehayas, N. (2006). A powered lift design for subsonic civil transport aircraft. In *Proceedings of the 25th International Congress of Aeronautical Sciences* (pp. 1–10). Hamburg, Germany.

Kehayas, N. (2007). Aeronautical technology for future subsonic civil transport aircraft. *Aircraft Engineering and Aerospace Technology, 79*(6), 600–610. https://doi.org/10.1108/00022660710829791

Kehayas, N. (2011a). *Integrated aircraft.* United States Patent and Trademark Office, US Patent Application No: 13/064,521 Mar. 30, 2011; Publication No: US2011/0240804, Oct. 6, 2011.

Kehayas, N. (2011b). Propulsion system of a jet-flapped subsonic civil transport aircraft design. *AIAA Journal of Aircraft*, *48*(2), 697–702. https://doi.org/10.2514/1.C031123

Kehayas, N. (2021). An alternative approach to induced drag reduction. *Aviation, 25*(3), 202–210. https://doi.org/10.3846/aviation.2021.15663

Kim, H. D., & Saunders, J. D. (2003). *Embedded wing propulsion conceptual study*. NASA TM-212696.

Kim, H. D., Berton, J. J., & Jones, S. M. (2006). Low noise cruise efficient short take-off and landing transport vehicle study. In *6th AIAA Aviation Technology, Integration and Operations Conference (ATIO),* AIAA 2006-7738, (pp. 1–11). Wichita, Kansas, USA. https://doi.org/10.2514/6.2006-7738

Ko, A., Schetz, J. A., & Mason, W. H. (2003). Assessment of the potential advantages of distributed propulsion for aircraft. In *16th International Symposium on Air Breathing Engines, ISABE-2003-1094* (pp. 1–9). Cleveland, Ohio, USA.

Kroo, I. (2001). Drag due to lift: Concepts for prediction and reduction. *Annual Review of Fluid Mechanics, 33*, 587–617. https://doi.org/10.1146/annurev.fluid.33.1.587

Lv, P., Rao, A. G., Ragni, D., & Veldhuis, L. (2016). Performance analysis of wake and boundary-layer ingestion for aircraft design. *Journal of Aircraft, 53*(5), 1517–1526. https://doi.org/10.2514/1.C033395

Leifsson, L. T., Ko, A., Mason, W. H., Schetz, J. A., Hatfka, R. T., & Grossman, B. (2005). *Multidisciplinary design optimization for a blended wing body transport aircraft with distributed propulsion.* Virginia Polytechnic Institute & State University Multidisciplinary Analysis and Design Center (MAD Center) Report 2005-05-01.

OXIS Energy. (2020). Next generation battery technology. In *Press Release, 22nd January 2020.* https://www.0xisenergy.com

Pfenninger, W., & Groth, E. (1961). Low drag boundary layer suction experiments in flight on a wing glove of an F-94A airplane with suction through a large number of fine slots. In G. V. Lachmann (Ed.), *Boundary layer and flow control* (Vol. 2, pp. 981–999). Pergamon Press. https://doi.org/10.1016/B978-1-4832-1323-1.50014-2

Reneaux, J. (2004). Overview of drag reduction technologies for civil transport aircraft. In P. Neittaanmaki, T. Rossi, S. Korotov, E. Oñate, J. Périaux, & D. Knörtzer (Eds), *European Congress on Computational Methods in Applied Sciences and Engineering (ECCOMAS 2004)* (pp. 1–18). Jyvädkylä, Finland.

Schetz, J. A., Hosder, S., Dippold III, V., & Walker, J. (2010). Propulsion and aerodynamic performance evaluation of jet-wing distributed propulsion. *Aerospace Science and Technology, 14*(1), 1–10. https://doi.org/10.1016/j.ast.2009.06.010

Smith, A. M. O., & Roberts, H. E. (1947). The jet airplane utilizing boundary layer air for propulsion. *Journal of the Aeronautical Sciences, 14*(2), 97–109. https://doi.org/10.2514/8.1273

Smith, L. H. (1993). Wake ingestion propulsive benefit. *Journal of Propulsion and Power, 9*(1), 74–82. https://doi.org/10.2514/3.11487

The Faraday Institution. (2020). *Faraday insights* (issue 8). https://www.faraday.ac.uk

Torenbeek, E. (2013). *Advanced aircraft design. Conceptual design, analysis and optimization of subsonic civil airplanes*. Wiley. https://doi.org/10.1002/9781118568101

Appendix A. Calculations for power balance and mass flow applied to wings

To find the power required in applying the laminar flow, propulsive, jet-flapped concept to wings, the kinetic and momentum thicknesses and Oswald factor must be calculated, and the efficiency of the system and the lift coefficient must be established.

Values for density and dynamic viscosity at 36,000 ft of 0.3652 kg/m^3 and 1.433 10^{-5} Pa s, and values for cruising speed and mean net aerodynamic chord of Table 1 lead to kinetic and momentum thicknesses of:

$$k = 1.044 \cdot \left(\frac{1.433 \cdot 3.187}{0.3652 \cdot 230} \right)^{1/2}; \quad \text{(A1)}$$

$$\theta = 0.664 \cdot \left(\frac{1.433 \cdot 3.187}{0.3652 \cdot 230} \right)^{1/2}; \quad \text{(A2)}$$

$$k = 7.7 \cdot 10^{-4}\, m; \quad \text{(A3)}$$

$$\theta = 4.897 \cdot 10^{-4}\, m. \quad \text{(A4)}$$

The Oswald factor calculated according to Howe (2000) is 0.89. Assuming system propulsion efficiency of 0.80, typical lift coefficient of 0.37 and using values for the rest of the parameters of Eq. (10) from Table 1, we can solve for the "equivalent drag" coefficient:

$$C_{DS} = \left(\frac{0.80}{2 \cdot 102} \right) \cdot \left(4 \cdot 32 \cdot 4.897 \cdot 10^{-4} + \frac{0.37^2 \cdot 123}{0.89 \cdot 3.14 \cdot 10.42} \right); \quad \text{(A5)}$$

$$C_{DS} = 25.135 \cdot 10^{-} \ . \quad \text{(A6)}$$

We can now calculate the terms of the power balance equation (Eq. (8)) applied to wings for cruising conditions at 36,000 ft:

$$\frac{25.135 \cdot 10^{-4} \cdot 0.5 \cdot 0.3652 \cdot 230^3 \cdot 2 \cdot 102}{0.8} =$$
$$32 \cdot 0.3652 \cdot 230^3 \cdot 7.7 \cdot 10^{-4} +$$
$$32 \cdot 0.3652 \cdot 230^3 \cdot \left(2 \cdot 4.897 - 7.7 \right) \cdot 10^{-4} +$$
$$\frac{0.37^2 \cdot 0.5 \cdot 0.3652 \cdot 230^3 \cdot 123}{0.89 \cdot 3.14 \cdot 10.42}; \quad \text{(A7)}$$

$$1{,}423{,}976\ W =$$
$$109{,}485\ W + 29{,}774\ W + 1{,}284{,}711\ W. \quad \text{(A8)}$$

Using Eqs (11) and (A6) leads to:

$$C_W = 0.65 \cdot 25.135 \cdot 10^{-4} + 0.5 \cdot 10^{-4}; \quad \text{(A9)}$$

$$C_W = 16.8378 \cdot 10^{-4} \quad \text{(A10)}$$

and from Eq (13) the mass flow rate, $\dot{m}_W$, is:

$$\dot{m}_W = 16.8378 \cdot 10^{-4} \cdot 230 \cdot 0.3652 \cdot 2 \cdot 102; \quad \text{(A11)}$$

$$\dot{m}_W = 28.8519 \frac{kg}{s}. \quad \text{(A12)}$$

Appendix B. Calculations for power balance and mass flow applied to wings with combined elliptical and astroid hypocycloid lift distribution

The only difference as opposed to the calculation for the usual elliptical lift distribution wings (Appendix A) is that induced drag is reduced by 50%. Therefore, using Eqs (A3) and (A4):

$$k = 7.7 \cdot 10^{-4}\, m; \quad \text{(B1)}$$

$$\theta = 4.897 \cdot 10^{-4}\, m \quad \text{(B1)}$$

and

$$C_{DS} = \left(\frac{0.80}{2 \cdot 102} \right) \cdot \left(4 \cdot 32 \cdot 4.897 \cdot 10^{-4} + 0.50 \cdot \frac{0.37^2 \cdot 123}{0.89 \cdot 3.14 \cdot 10.42} \right); \quad \text{(B3)}$$

$$C_{DS} = 13.7964 \cdot 10^{-4}. \quad \text{(B4)}$$

We can now calculate the terms of the power balance equation (Eq. (8)) applied to wings with combined

elliptical and astroid lift distribution for cruising conditions at 36,000 ft:

$$\frac{13.7964\cdot10^{-4}\cdot0.5\cdot0.3652\cdot230^3\cdot2\cdot102}{0.8}=$$

$$32\cdot0.3652\cdot230^3\cdot7.7\cdot10^{-4}+$$

$$32\cdot0.3652\cdot230^3\cdot\left(2\cdot4.897-7.7\right)\cdot10^{-4}+$$

$$0.50\frac{0.37^2\cdot0.5\cdot0.3652\cdot230^3\cdot123}{0.89\cdot3.14\cdot10.42}; \quad \text{(B5)}$$

$$781{,}610\ W=$$

$$109{,}485\ W+29{,}774\ W+642{,}355\cdot \quad \text{(B6)}$$

Using Eqs (11) and (B4) leads to:

$$C_W=0.65\cdot13.7964\cdot10^{-4}+0.5\cdot10^{-4}; \quad \text{(B7)}$$

$$C_W=9.4677\cdot10^{-4} \quad \text{(B8)}$$

and from Eq. (13) the mass flow rate, $\dot{m}_W$, is:

$$\dot{m}_W=9.4677\cdot10^{-4}\cdot230\cdot0.3652\cdot2\cdot102; \quad \text{(B9)}$$

$$\dot{m}_W=16.2231\frac{kg}{s}. \quad \text{(B10)}$$

Appendix C. Calculations for power balance and mass flow applied to fuselage

To find the power required in applying the laminar flow, propulsive concept to fuselage, the kinetic and momentum thicknesses must be calculated, and the efficiency of the system must be established.

Assuming flat plate conditions, the length of the fuselage as the characteristic length, values for density and dynamic viscosity at 36,000 ft of 0.3652 kg/m^3 and 1.433 10^{-5} Pa s, and values for cruising speed and fuselage length of Table 1 lead to kinetic and momentum thicknesses of:

$$k=1.044\cdot\left(\frac{1.433\cdot37.57}{0.3652\cdot230}\right)^{1/2}; \quad \text{(C1)}$$

$$\theta=0.664\cdot\left(\frac{1.433\cdot37.57}{0.3652\cdot230}\right)^{1/2}; \quad \text{(C2)}$$

$$k=2.6434\cdot10^{-3}m; \quad \text{(C3)}$$

$$\theta=1.6812\cdot10^{-3}m\cdot \quad \text{(C4)}$$

Assuming again system propulsion efficiency of 0.80 and using values for the rest of the parameters of Eq. (18) from Table 1, we can solve for the "equivalent drag" coefficient:

$$C_{DS}=0.80\cdot\left(\frac{4\cdot1.6812\cdot10^{-3}}{37.57}\right); \quad \text{(C5)}$$

$$C_{DS}=1.4319\cdot10^{-4}. \quad \text{(C6)}$$

We can now calculate the terms of the power balance equation (Eq. (16)) applied to fuselage for cruising conditions at 36,000 ft:

$$\frac{1.4319\cdot10^{-4}\cdot0.5\cdot0.3652\cdot230^3\cdot420}{0.80}=$$

$$\frac{420}{37.57}\cdot0.3652\cdot230^3\cdot2.6434\cdot10^{-3}+$$

$$\frac{420}{37.57}\cdot0.3652\cdot230^3\cdot\left(2\cdot1.6812-2.6434\right)\cdot10^{-3}; \quad \text{(C7)}$$

$$167{,}015W=131{,}306W+35{,}715W. \quad \text{(C8)}$$

Using Eqs (11) and (C6) leads to:

$$C_W=0.65\cdot1.4319\cdot10^{-4}+0.5\cdot10^{-4}; \quad \text{(C9)}$$

$$C_W=1.4307\cdot10^{-4} \quad \text{(C10)}$$

and from Eq. (20) the mass flow rate, $\dot{m}_F$, is:

$$\dot{m}_F=1.4307\cdot10^{-4}\cdot230\cdot0.3652\cdot42; \quad \text{(C11)}$$

$$\dot{m}_F=5.0474\frac{kg}{s}. \quad \text{(C12)}$$

Appendix D. Calculations for the specific energy of the electric storage system

Following section 3.1. the energy consumed by the aircraft during the flight is:

- Energy consumed by AC(WE + F) = 2,088,176 · 3.6 + (100/70) · 2,088,176 · (0.6981/0.3652) · 0.6 = 10,938,764 Wh
- Energy consumed by AC(WE + F + T) = (2,088,176 + 0.35 · 1,423,970) · 3.6 + (100/70) · (2,088,176 + 0.35 · 1,423,970) · (0.6981/0.3652) · 0.6 = 13,549,539 Wh
- Energy consumed by AC(WC + F) = 1,245,084 · 3.6 + (100/70) · 1,245,084 · (0.6981/0.3652) · 0.6 = 6,522,283 Wh
- Energy consumed by AC(WC + F + T) = (1,245,084 + 0.35 · 781,614) · 3.6 + (100/70) · (1,245,084 + 0.35 781,614) · (0.6981/0.3652) · 0.6 = 7,955,334 Wh

Therefore, following section 3.1. the specific energy of the electrical energy storage system must be:

- Specific energy for AC(WE + F) = 10,938,764/9,756 = 1,121 Wh/kg
- Specific energy for AC(WE + F + T) = 13,549,539/9,756 = 1,389 Wh/kg
- Specific energy for AC(WC + F) = 6,522,283/9,756 = 668 Wh/kg
- Specific energy for AC(WC + F + T) = 7,955,334/9,756 = 815 Wh/kg

Appendix E. Calculations for the specific power of the electric storage system

Following section 3.2. the maximum power required by the aircraft is:

- Maximum power required by AC(WE + F) = (100/70) · 2,088,176 · (1.225/0.3652) = 10,006,320 W
- Maximum power required by AC(WE + F + T) = (100/70) · (2,088,176 + 0.35 · 1,423,970) · (1.225/0.3652) = 12,409,644 W

– Maximum power required by AC(WC + F) = (100/70) · 1,245,084 · (1.225/0.3652) = 5,966,312 W
– Maximum power required by AC(WC + F + T) = (100/70) · (1,245,084 + 0.35 · 781,614) · (1.225/0.3652) = 7,277,225 W

Consequently, following section 3.2. the specific power of the electrical energy storage system must be:

– Specific power for AC(WE + F) = 10,006,320/12,350 = 810 W/kg
– Specific power for AC(WE + F + T) = 12,409,644/12,350 = 1,005 W/kg
– Specific power for AC(WC + F) = 5,966,312/12,350 = 483 W/kg
– Specific power for AC(WC + F + T) = 7,277,225/12,350 = 589 W/kg

Appendix F. Calculations for the mass of the electric motors

According to section 4:

– Mass of electric motors for AC(WE + F) = 10,006,320/3,308 = 3,025 kg
– Mass of electric motors for AC(WE + F + T) = 12,409,644/3,308 = 3,751 W/kg
– Mass of electric motors for AC(WC + F) = 5,966,312/3,308 = 1,804 W/kg
– Mass of electric motors for AC(WC + F + T) = 7,277,225/3,308 = 2,200 W/kg

Notations

AR – wing aspect ratio;
b_N – net (exposed) wingspan (m);
C_{DS} – "equivalent drag" coefficient;
c_N – mean net aerodynamic wing chord (m);
C_L – lift coefficient;
C_W – weight flow coefficient;
d_m – mean geometric fuselage diameter (m);
e – Oswald factor;
F_X – force on the wing (N);
k – kinetic thickness (m);
l – fuselage length (m);
$\dot{m}_{WC}$ – mass flow rate for wing – combined lift distribution (kg/s);
$\dot{m}_F$ – mass flow rate for fuselage (kg/s);
$\dot{m}_W$ – mass flow rate for wing (kg/s);
P_{FK} – mechanical flow power for fuselage (W);
P_{WK} – mechanical flow power for wing – combined lift distribution (W);
P_{WK} – mechanical flow power for wing (W);
S – wing reference surface (m^2);
S_F – fuselage wetted surface (m^2);
S_N – net (exposed) wing surface (m^2);
U_0 – undisturbed flow velocity – flight speed (m/s);
U_{in} – velocity of suction air in the direction of flight (m/s);
U_j – engine jet velocity (m/s);
η – efficiency of the system;
θ – momentum thickness (m);
μ – dynamic viscosity (Pa s);
ρ – air density (kg/m^3);
Φ_{fej} – energy dissipation of the engines jet – fuselage (W);
Φ_{fs} – energy dissipation in the fuselage surface (W);
Φ_{fv} – energy dissipation of the fuselage vortices (W);
Φ_{fw} – energy dissipation of the fuselage wake (W);
$\Phi_{f\infty}$ – total fuselage energy dissipation (W);
Φ_{wcs} – energy dissipation in the wing surface boundary layer – combined lift distribution (W);
Φ_{wcv} – energy dissipation of the wing vortices – combined lift distribution (W);
Φ_{wcw} – energy dissipation of the wing wake – combined lift distribution (W);
Φ_{wej} – energy dissipation of the engines jet – wing (W);
Φ_{ws} – energy dissipation in the wing surface boundary layer (W);
Φ_{wv} – energy dissipation of the wing vortices (W);
Φ_{ww} – energy dissipation of the wing wake (W);
Φ_{fej} – energy dissipation of the engines jet – fuselage (W);
$\Phi_{w\infty}$ – total wing energy dissipation (W).

Abbreviations

AC/WE + F – Aircraft with elliptical wing lift distribution and fuselage without a tail;
AC/WE + F + T – Aircraft with elliptical wing lift distribution and fuselage with a tail;
AC/WC + F – Aircraft with combined wing lift distribution and fuselage without a tail;
AC/WC + F + T – Aircraft with combined wing lift distribution and fuselage with a tail.